



Enhancing adaptability with local reactive behaviors for hexapod walking robot via sensory feedback integrated central pattern generator

Haitao Yu ^{a,b,*}, Haibo Gao ^a, Zongquan Deng ^a

^a State Key Laboratory of Robotics and Systems, Harbin Institute of Technology, Harbin, 150080, China

^b State Key Lab of Digital Manufacturing Equipment and Technology, Huazhong University of Science and Technology, Wuhan, 10487, China



ARTICLE INFO

Article history:

Received 13 July 2019

Received in revised form 18 October 2019

Accepted 4 December 2019

Available online 9 December 2019

Keywords:

Hexapod walking robot

Legged locomotion

Local reactive behavior

Central pattern generator (CPG)

ABSTRACT

Local reactive behaviors endow animals the ability to exhibit agile and dexterous performance when traversing challenging terrains. This paper presents a novel locomotion control method based on the central pattern generator (CPG) concept for hexapod walking robot with local reactive behavior to cope with terrain irregularities. Firstly, a two-layered CPG-based single-leg controller is developed to generate the rhythmical movement for each leg executing tripod walking. The Van der Pol oscillator is employed on the high-layer to construct a coupled CPG network which serves as a phase regulator (PR) to produce rhythmic signals with prescribed phase relations amongst neurons. On the low-layer, an auxiliary linear converter (LC) transforms these signals into the desired joint trajectories. Subsequently, by embodying the proprioceptive sensing and external tactile information as the sensory feedback, two typical local reactive mechanisms including the elevator reflex and searching reflex are achieved by virtue of on-line adjusting the coupling scheme of the PR and the coefficients of the LC. A locomotion control framework for hexapod walking robot is further established by combining the single-leg controller with a finite state machine to allocate swing/stance commands for individual joints in dealing with terrain perturbations. The effectiveness of the proposed method has been verified through both virtual model simulation and experiments on a physical hexapod platform.

© 2019 Elsevier B.V. All rights reserved.

1. Introduction

Achieving agile and robust walking performance as presented in vertebrates and arthropods becomes increasingly attractive for legged robots when traversing complicated terrains in recent years [1–3]. Due to the inherent redundancy among the joints and the complexity in foot-ground interaction, tackling the motion coordination of multi-degrees of freedom (MDoF) and multi-axial movement is regarded as a challenge in locomotion control of legged robots [4]. The relevant biological observations and experimental results provide abundant inspirations for scientists and engineers to deal with this issue. By refining the essence of the neuro-mechanics, a series of legged prototypes such as RHex [5], Zebro [6], Foldable Hexapod [7], PhantomX [8], HITCR-II [9], Octopus-III [10] and AMOS [11] have been successfully developed, exhibiting astonishing adaptive behaviors in varied surfaces. Recently the desert ant-inspired 3D printed hexapod robots [12] have been devised and provided an affordable alternative in outdoor exploration due to the distinctive

adaptability in unknown environment [13,14]. With regard to traversing rough terrains, a position feedback-based adaptive locomotion control method has been proposed in [15] for affordable hexapod walking robot to improve the mobility in typical unstructured terrains (i.e., stairs, irregular blocks). Nonetheless, the underlying mechanism on how animals maneuver tissues, organs as well as limbs to produce energetically efficient and dexterously movements when interacting with the unstructured environment still remains unsettled.

Recent neuroscience research has found that the central pattern generator (CPG), a group of neural circuit located in the spinal cord of vertebrates or in relevant ganglia in invertebrates, can produce rhythmic and quasi-periodic movement in absence of sensory feedback or higher regulation signals from the brain-stem level [16]. Meanwhile, the neurobiology studies [17–19] have revealed that the local reactive behaviors via muscles, tissues and organs with tactile sensing or vestibular feedback plays an irreplaceable role for terrestrial creatures when coping with unconventional environment. These biological observations and findings inspire both engineers and roboticists to resolve specific locomotory tasks for legged robots. Lewinger et al. [20] proposed a biologically inspired leg controller to generate adaptive stepping actions in a hexapod walking robot. The proposed controller

* Corresponding author at: State Key Laboratory of Robotics and Systems, Harbin Institute of Technology, Harbin, 150080, China.

E-mail address: yht@hit.edu.cn (H. Yu).

contains three sensory-coupled neuron circuits by collecting the angle and load information of each joint, exhibiting a motion combination including the protraction of the thorax-coxa, the elevation of the coxa-trochanter as well as the extension of the femur-tibia. Rutter et al. [21] extended this work by developing a neural network-based single-leg controller with local sensor feedback to steer a cockroach-like robotic leg. By appropriately inhibiting or exciting the local neural circuits and adjusting the associated neuron thresholds, a series of adaptive reflex transitions were obtained on the single-leg platform. Similar results could be found in [22] wherein the movement of a 3-DoF leg is steered by the proposed joint controller that embodies simplified linear muscle models. The strategy based on bio-inspired local reactive behavior was also implemented in [23] that the reactive climbing performance for hexapod walking robot AMOS-II is conducted via the central pattern generator (CPG) network integrated with reflex neurons. The robot could negotiate obstacles with varied height, displaying a comparable climbing behaviors as observed in cockroaches. The reflex mechanism had also been cooperated with the CPG network to successfully manipulates a limbless robot for improving adaptability in unstructured environment with rapid response in presence of external stimuli [24]. Kimura et al. [25] developed a CPG-based controller for the quadruped prototype Tekken-II in which the corrective stepping reflex together with the crossed flexor reflex induced by sensory feedback was implemented on the swing leg to maintain the balance when dynamically walking on irregular terrain in outdoor environment. Wang et al. [26] also achieved stable and robust hopping for a biped robot in uneven surface by elaborately adding sensory feedback path to the original CPG circuits. Espenschied et al. [27] proposed a distributed locomotion controller incorporating with local leg reactive behaviors including step reflex, elevator reflex as well as searching behaviors for a insect-like hexapod robot to enhance the walking adaptation when negotiating complicated terrains such as irregular, slatted and compliant surface.

Although these bio-inspired reflex control methods are widely and fruitfully applied in locomotion control of legged robots, it still remains a challenge for locomotion control of legged robots that how to generate suitable and efficient reactive behaviors comparable to natural performance of animals. Generally, constructing the CPG network for locomotion control is a trade-off between the complexity of the neural network topology and the diversity of the resulting gait patterns. From the perspective of synchronization of complex network, the rhythmical signals with stable phase relationships that are appropriate to generate diverse gait patterns for legged locomotion depends on the collective dynamical behaviors of the CPG network with specific coupling scheme amongst neurons. However, the sophisticated topology of the CPG network will inevitably reduce the mathematical tractability, which further decreases the possibility of straight-forward parametrical synthesis of the CPG-based controller for locomotory tasks in steering limb/limbless movement. Traditional numerical methods such as evolutionary searching [28], empirical tuning [29] as well as other learning approaches [30,31] are applied to obtain the appropriate model parameters of the neural network. Constructing an ideal CPG network capable of providing abundant dynamical behaviors that results rhythmic locomotion patterns meanwhile preserving tractability is a long-term goal for the CPG-based locomotion control for legged robots especially in cope with unstructured terrain profiles.

Aiming at improving the adaptability of hexapod walking robot in unstructured environment, this paper presents a novel CPG-based locomotion controller with sensory feedback to generate local reactive behaviors for single-leg in dealing with irregular

terrain. To fully leverage the merit of the CPG-based approach in producing rhythmic signals with stable phase relationships among neurons, a coupled neuron network integrating with proprioceptive sensing and external tactile information to exhibit conventional leg movement in tripod gait and two typical adaptive reactive behaviors. The main contributions of this paper are summarized as follows.

1. A two-layered CPG-based single-leg controller is developed to generate reference trajectory for hexapodal walking in conventional tripod gait. On the high-level, the CPG network composed of three coupled Van der Pol oscillators is constructed as the phase regulator (PR) to produce rhythmic signals with prescribed waveforms. These signals are transformed into the desired joint trajectories for a single-leg by using a linear convertor (LC) on the low-level.
2. Two typical local reactive behaviors including the elevator reflex and searching reflex are achieved by adjusting the coupling scheme of the PR and the coefficients of the LC. The former reflex mainly deals with irregular terrain (i.e., step obstacles) to avoid stumbling while the latter treats sunk terrain (i.e., gap, ditches or holes) to search feasible foothold.
3. A comprehensive locomotion control framework for hexapod walking robot by combining the single-leg controller with two reflex mechanisms is established by using a finite state machine (FSM) to schedule individual legs in swing/stance phase during walking. The effectiveness of the proposed method is demonstrated through the simulation on a virtual hexapod model and the experiments on physical hexapod robot.

The remainder of this paper is organized as follows. Section 2 briefly revisits the neurobiological basis of the motor system in animals. Section 3 presents the development of the CPG-based single-leg controller with sensory feedback. Reactive behavior generation is detailed in Section 4 followed by the establishment of locomotion control framework for hexapod robot in Section 5. The effectiveness of the proposed controller is validated via both simulation and experiments in Section 6. The paper ends with conclusions in Section 7.

2. Neurobiological basis of the motor system in animals

It is an undeniable fact that the distinguished walking performance of animals outperforms any man-made legged devices at present. This section briefly revisits the essential features of the motor system that contribute to generate rhythmic movement with reactive behaviors. Fig. 1 illustrates the essential features of the motor system in animals by highlighting three pathways of feedback, namely, the central feedback, the reflex feedback and the sensory feedback [32].

The rhythmic movement of animals can be modulated by either high control command from brain-stem level or sensory feedback from the environment. Consequently, the effector organs will produce corresponding response according to the motor pattern generated by the CPG in order to overcome the unexpected environmental disturbance. In this paper, we focus on integrating the sensory feedback (i.e., tactile sensing) into the ordinary CPG-based control loop while the robot interacts with external environment. With the help of these information, two reactive mechanisms including the elevator reflex and searching reflex will be developed in the following sections. Note that these reactive behaviors are observed in the biology experiments on insects [33–36]. According to the walking testing on locust implemented by Pearson et al. [36], the elevator reflex is triggered when the leg hits on step obstacle in swing phase. The involved

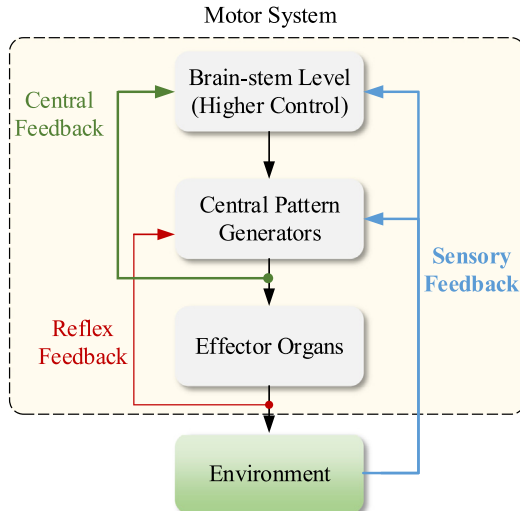


Fig. 1. The schematic of the key features of the motor system with feedback pathways in animals.
Source: Adapted from [32].

swing-leg usually lifts up to generate a higher ground clearance so as to negotiate. Another reactive behavior is called the searching behavior triggered in absent of foothold when the leg approaches at the end of the nominal swing phase. Apparently, sunk terrain profiles such as gaps, ditches and holes are apt to trigger this behavior. Cruse et al. studied stick insects walking on irregular terrain and found that hind-leg seeks foothold site around support site of fore-leg when traversing ditches [35]. Pearson et al. observed that locusts accelerate movements of elevation and depression via lengthening swing phase to explore border space for several cycles and terminate when new available ground support is reattain [36].

3. CPG-based single-leg controller with sensory feedback

3.1. The neuron model

The CPG network is modeled as a group of coupled nonlinear neurons. We hereby introduce the classical Van der Pol (VDP) oscillator as the elementary neuron with

$$\ddot{x} + \varepsilon(bx^2 - 1)\dot{x} + \omega_0^2 = 0, \quad (1)$$

where ω_0 is the oscillation frequency, ε is a scalar coefficient quantifying the strength of the nonlinear damping ($0 < \varepsilon \ll 1$) and b is the amplitude adjustment parameter. We rewrite the VDP model into the state-space formulation as

$$\dot{\mathbf{z}} = \mathbf{F}(\mathbf{z}) = \begin{bmatrix} \dot{x} \\ \dot{y} \end{bmatrix} = \begin{bmatrix} y \\ \varepsilon(1 - bx^2)y - \omega_0^2x \end{bmatrix}, \quad (2)$$

where $\mathbf{z} = [x, y]^T$ is the state vector of the VDP oscillator. Unfortunately, the exact solution of (1) does not exist due to the nonlinear damping term. As an alternative, one may seek an analytical approximation via the perturbation approach (i.e., the method of multiple scales) to derive the 1st-order expression as

$$x \approx \frac{2}{\sqrt{b + \left(\frac{4}{\omega_0^2} - b\right)e^{-\varepsilon t}}} \cos(\omega_0 t + \phi_0), \quad (3)$$

where a_0 and ω_0 are determined by the initial condition. The steady-state solution of (3) can be further derived via $t \rightarrow \infty$

as

$$\begin{cases} x_\infty = \frac{2}{\sqrt{b}} \cos(\omega_0 t + \phi_0) \\ y_\infty = -\frac{2\omega_0}{\sqrt{b}} \sin(\omega_0 t + \phi_0) \end{cases} \quad (4)$$

It is obvious to see that the amplitude, natural frequency of the VDP output can be independently maneuvered by tuning the parameter b and ω_0 . Hereafter, the steady-state solution (4) will be employed to formulate the limit cycle behavior of the VDP, which will facilitate the coupled CPG network design of the single-leg controller in the following section.

3.2. Two-layered single-leg controller

The local coordinate system of single-leg $\{x_L, y_L, z_L\}$ are setup with respect to the body as shown in Fig. 2. The arrow located at each joint marks the positive rotary direction. In this paper, the single-leg movement in tripod gait pattern is regarded as three coupled rhythmic waveforms with specific phase relationships. Thereby the single-leg controller consists of two levels, namely the phase regulator (PR) as the high-level and the linear converter (LC) as the low-level. The PR contains three coupled neuron oscillators that output periodic sinusoidal waveforms with fixed phase lags among the neurons. The LC transfers these coupled signals directly into the desired joint trajectory of each leg. In this manner, the rhythmic movement of the 3-DoF leg on flat surface can be understood as a group of periodic trajectories with specified phase and amplitude relationship. Consequently, the output of the CPG network can be decoupled from the kinematical constraints of the hexapod robot.

The dynamics of the CPG network with three coupled neurons is given by

$$\begin{cases} \dot{x}_1 = y_1 \\ \dot{y}_1 = -\varepsilon_1(b_1x_1^2 - 1)y_1 - \omega_1^2x_1 \\ \dot{x}_2 = y_2 \\ \dot{y}_2 = -\varepsilon_2(b_2x_2^2 - 1)y_2 - \omega_2^2x_2 + k_{12}(-4y_1x_1 - y_2) \\ \quad + k_{32}(y_3 - y_2) \\ \dot{x}_3 = y_3 \\ \dot{y}_3 = -\varepsilon_3(b_3x_3^2 - 1)y_3 - \omega_3^2x_3 + k_{13}(-4y_1x_1 - y_3) \\ \quad + k_{23}(y_2 - y_3) \end{cases} \quad (5)$$

where $x_i (i = 1, 2, 3)$ is the state of the i th neural oscillator, b_i , ε_i , ω_i are the corresponding structure parameters of the VDP model and k_{ij} is the connection strength between the i th and the j th neural oscillator.

The coupling scheme in (5) forms a *leader-follower* network where \mathbf{z}_1 serves as the leader neuron to regulate α -joint (body-coxa joint), and \mathbf{z}_2 , \mathbf{z}_3 serve as the follower neuron to take charge of β -joint (coxa-femur joint) and γ -joint (femur-tibia joint) respectively. The leader neuron can be considered as an isolated node, obviously the evolution of which could not be influenced by other two nodes. Note that there are two categories of the coupling terms in each follower neuron \mathbf{z}_2 and \mathbf{z}_3 . The first coupling term $k_{1i}(-4x_1y_1 - y_i) (i = 2, 3)$ works as an external stimulus signal from the leader neuron \mathbf{z}_1 that drives each follower neuron to oscillate at the frequency of $2\omega_1$. The second coupling term $k_{ij} (y_i - y_j)$ works as a mutual connection that synchronizes the rhythmic oscillation between \mathbf{z}_2 and \mathbf{z}_3 .

The linear converter that transfers the generated coupled neural signals into the joint trajectory for each leg is formulated by

$$\begin{cases} \alpha = \mathbf{G}_1(\mathbf{z}_1) = g_\alpha x_1 + h_\alpha \\ \beta = \mathbf{G}_2(\mathbf{z}_2) = g_\beta x_2 + h_\beta \\ \gamma = \mathbf{G}_3(\mathbf{z}_3) = g_\gamma x_3 + h_\gamma \end{cases} \quad (6)$$

where $g_\alpha, g_\beta, g_\gamma$ are the amplitude coefficients of the α -, β - and γ -joint, respectively. $h_\alpha, h_\beta, h_\gamma$ are the offset coefficients

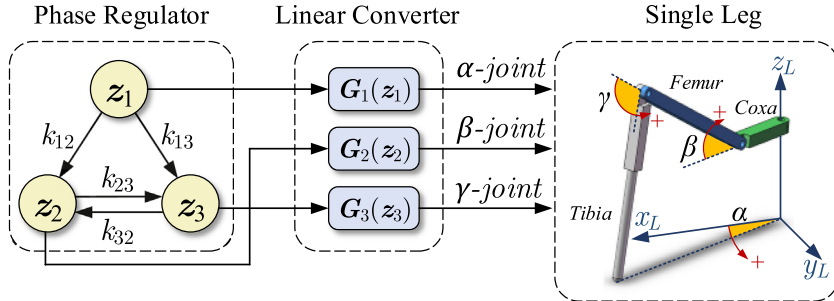


Fig. 2. Schematic of the two-layered single leg controller.

Table 1
Parameters of the CPG network.

Symbol	Value	Descriptions
$\varepsilon_1, \varepsilon_2, \varepsilon_3$	0.1	Nonlinear coupling coefficient of VDP
b_1, b_2, b_3	4	Amplitude coefficient of VDP
$\omega_1, \omega_2, \omega_3$	$0.4\pi, 0.8\pi, 0.8\pi$	Natural frequency of VDP
$k_{12}, k_{13}, k_{23}, k_{32}$	0.1	Connection weight of the neurons

correspondingly. Owing to the dual sub-phases (i.e., swing and stance phase) in leg movement of the gait cycle, two groups of the coefficients are applied in generating the desired joint trajectory for the three-segmented leg, namely, $\{g_\alpha^{st}, g_\beta^{st}, g_\gamma^{st}, h_\alpha^{st}, h_\beta^{st}, h_\gamma^{st}\}$ for stance phase and $\{g_\alpha^{sw}, g_\beta^{sw}, g_\gamma^{sw}, h_\alpha^{sw}, h_\beta^{sw}, h_\gamma^{sw}\}$ for swing phase.

Given the explicit expression of the CPG network (5) and the linear converter (6), the specific movement of the single-leg can be further determined. Taken the kinematical information of the hexapod robot into consideration, the corresponding parameters of the CPG network are collected in Table 1. Note that the amplitude of each neuron model is deployed to unity with $b_i = 4$ for $i = 1 \sim 3$. The traditional tripod gait is of interest for hexapodal walking in this paper such that the entire gait cycle is equally divided by the swing phase and stance phase, which implies that the frequency of three neurons that governs individual joints satisfy $\omega_1 : \omega_2 : \omega_3 = 1 : 2 : 2$.

According to the kinematical constraint of the robotic leg, the range of α -joint (body-coxa joint) is bounded at $[-\pi/6, \pi/6]$. The movements of the remaining joint β and γ can be determined according to the ground clearance h_{max} and body support height with respect to the level ground H . Therefore, the coefficients in (6) for swing and stance phases can be easily obtained via calculating the inverse kinematics of the single-leg at the anterior extreme position (AEP), the posterior extreme position (PEP), apex as well as the stance midpoint of the foot trajectory.

Fig. 3 shows the numerical simulation result of the evolution of the CPG network. The initial condition of the network (5) is arbitrarily chosen. The leader neuron x_1 converges into periodic trajectory of the VDP limit cycle because it is an isolated node. Two follower neurons x_2 and x_3 reach the corresponding synchronous states with each other after roughly 2 s through the mutual coupling terms aforementioned. Furthermore, these two outputs x_2 and x_3 evolve with x_1 at the prescribed constant frequency ratio $\omega_1 : \omega_2 : \omega_3 = 1 : 2 : 2$, and the phase lag between x_1 and $x_2(x_3)$ maintains at $\pi/2$ as scheduled, providing a phase-locked property amongst the neurons. Fig. 4 shows the resulting limit cycles of individual joint trajectories in tripod gait. α -joint has just one limit cycle while β - and γ -joint possess two (each for the swing and stance phase, respectively). The single-leg controller outputs nearly constant AEP and PEP on flat terrain during hexapodal walking.

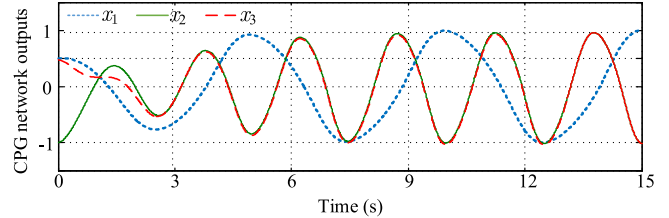


Fig. 3. Numerical simulation of the evolution of the CPG network.

3.3. Sensory feedback pathway

The sensory feedback pathway mainly transmits the contact information of the toe into the CPG network, providing a tactile feedback when the leg encounters external disturbances caused by irregular terrain profile such as step obstacle and ditches. The schematic of the sensory feedback pathway is shown in Fig. 5.

Without loss of generality, the contact force vector of the toe F_{toe} can be expressed as

$$\mathbf{F}_{toe} = [F_{toe-x}, F_{toe-y}, F_{toe-z}]^T \quad (7)$$

where F_{toe-x} , F_{toe-y} , F_{toe-z} denote the components in the lateral, forward and vertical direction (see Fig. 5 for details). The horizontal components F_{toe-x} and F_{toe-y} are utilized to detect the step obstacle in swing phase while the vertical component F_{toe-z} is utilized to judge whether the foot contacts with the surface as scheduled. Two sensory neurons (SN) are added to the sensory feedback pathway. Additionally, three pre-defined contact force thresholds for each component are introduced to guarantee the contact strength with terrain.

For the sensory neuron SN_{ob} to detect the step obstacle during the halfway of swing, the elevator reflex trigger signal is given by

$$\begin{aligned} \lambda_{ob} = & \text{sign}(\max(|F_{toe-x}| - F_{contact-x}, 0)) \\ & + \text{sign}(|F_{toe-y}| - F_{contact-y}, 0) \end{aligned} \quad (8)$$

where λ_{ob} is the elevator reflex trigger signal for swing-leg. $\text{sign}(\cdot)$ denotes the signum function and $F_{contact-x}$, $F_{contact-y}$ are the contact force detection thresholds in lateral and forward direction, respectively. Note that the value of λ_{ob} is in binary format to reveal whether ($\lambda_{ob} = 1$) or not ($\lambda_{ob} = 0$) the leg encounters the step obstacle.

For the sensory neuron SN_{td} to detect the foot touchdown at the end of swing, the searching reflex trigger signal is given by

$$\lambda_{td} = \text{sign}(\max(|F_{toe-z}| - F_{contact-z}, 0)) \quad (9)$$

where λ_{td} is the searching reflex trigger signal, $F_{contact-z}$ is the contact force detection threshold in vertical direction. Similar to λ_{ob} , λ_{td} is also a binary scalar where $\lambda_{td} = 0$ indicates the leg loses contact with ground and $\lambda_{td} = 1$ indicates the leg contacts with ground.

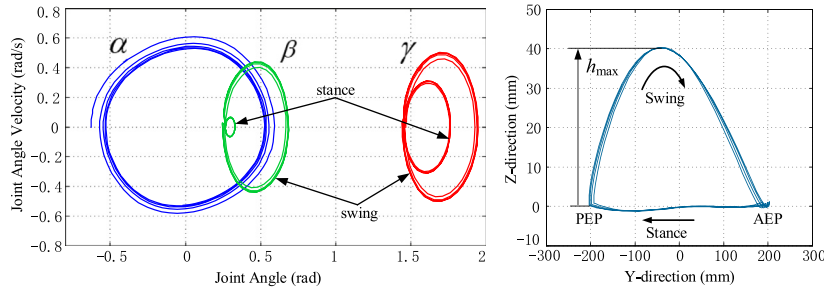


Fig. 4. Numerical results of the outputs of the single-leg controller with arbitrarily chosen initial value for the CPG network (see Section 6.1 for the structural specifications for the virtual hexapod model in simulation): (a) limit cycles on the phase portraits of individual joints during the tripod gait cycles, (b) the resulting nominal foot trajectory on the sagittal plane. In contrast to the α -joint that exhibits only one limit cycle, the β - and γ -joint contain two limit cycles (each for the swing and the stance phase, respectively) illustrated by the arrows. This is due to the different amplitude and offset coefficients used in (4) for the sub-phases in tripod gait. The arrows in (b) indicate the evolving direction of the foot trajectories over time.

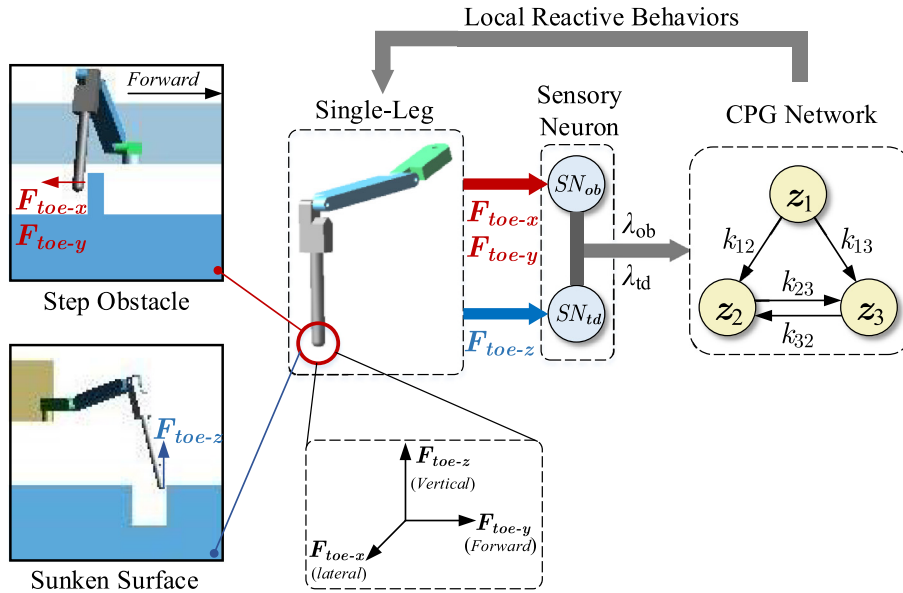


Fig. 5. The schematic of the sensory feedback pathway. The partial views illustrate two typical irregular terrain profiles (the upward disturbance as the step obstacle and the downward disturbance as the sunken surface) that the single-leg may encounter during the conventional gait cycles. Technically, the tactile sensing information F_{toe} of the toe will be transformed into the trigger signal λ_{ob} and λ_{td} in the sensory neuron SN_{ob} and SN_{td} (see Section 4 for details) to further switch the associated CPG network and the linear converter (see Section 5.1 for the switching mechanisms), resulting local reactive behaviors in dealing with unexpected terrain disturbances.

These two local reflex trigger signals will be transmitted into the CPG network (5), which will be presented in Section 5. The single-leg controller generates local reactive behaviors to cope with the terrain disturbance according to the signal λ_{ob} and λ_{td} .

4. Reactive behavior generation

4.1. Elevator reflex generation

The elevator reflex is activated when the step obstacle occurs during the halfway of the swing phase, provided that the obstacle is not too large to negotiate. For the single-leg control, the elevator reflex is switched on when the following conditions hold simultaneously.

- The single-leg is sweeping during the halfway of the swing phase, namely $\dot{x}_1 > 0$.
- The contact force components F_{toe-x} and F_{toe-y} satisfy $F_{toe-x} > F_{contact-x}$ or $F_{toe-y} > F_{contact-y}$.

To successfully pass through the step obstacle, the leg involved has to prolong its nominal swing duration so as to supply enough

time to accomplish the following actions: retract, lift up and then stretch as shown in Fig. 6 (Stage II). In the second stroke, the foot regenerates the path with a higher ground clearance \tilde{h}_{\max} .

The swing-leg trajectory can be regarded as a sub-segment of the limit cycle produced by (5). The trajectories with different ground clearances indicate different limit cycles in joint space. Thereby the elevator reflex could be illustrated in Fig. 6 (right). Stage I and II denote the original and updated swing trajectory, respectively. The elevator reflex acts as the transition curve that connects these two stages. The aforementioned reactive mechanism can be easily achieved on the two-layered single-leg controller presented in Section 3.2. On the high-level, the CPG network always outputs three synchronous rhythmic signals with prescribed frequencies and phase lags, preserving the waveforms that generates the nominal swing trajectory. On the low-level, the linear converter adjusts the coefficient to enlarge the ground clearance so that the leg could negotiate the obstacle. In order to execute the retraction, the leader neuron that governs the hip joint α has to reverse its oscillation direction since the elevator reflex is triggered on, which implies

$$\begin{cases} x_1(t_{ob}^+) = x_1(t_{ob}^-) \\ y_1(t_{ob}^+) = -1 \end{cases} \quad (10)$$

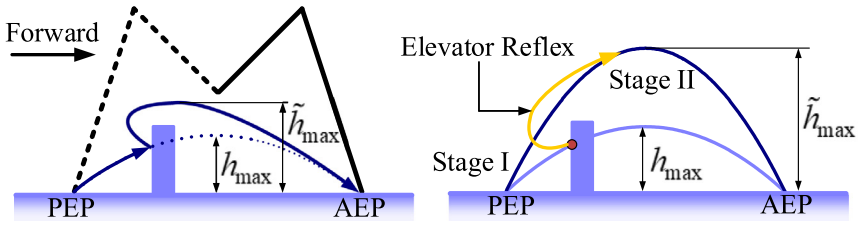


Fig. 6. The elevator reflex behavior when colliding with step obstacle. Trajectory of toe during reflex (left) and stage division (right). The transition curve between stage I and II is highlighted in yellow. (For interpretation of the references to color in this figure legend, the reader is referred to the web version of this article.) Source: Adapted from [27].

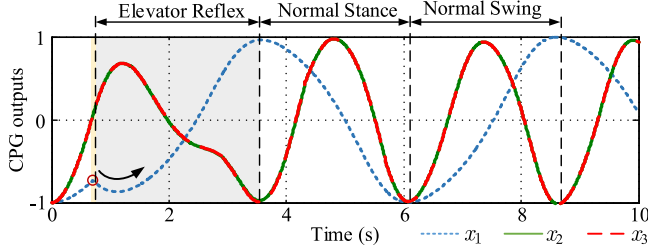


Fig. 7. Numerical result of the CPG network output in elevator reflex.

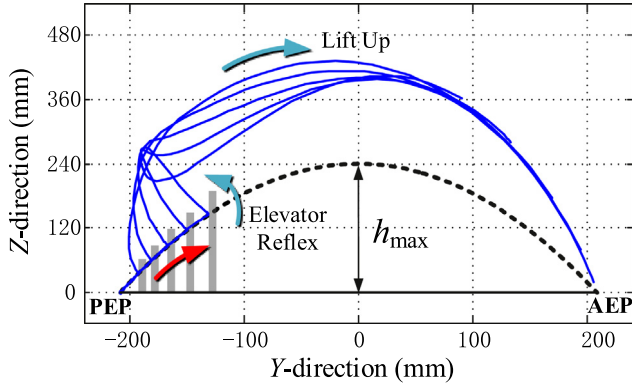


Fig. 8. Numerical result of the foot trajectory on sagittal plane during elevator reflex. See Section 6.1 for the structural specifications for the virtual hexapod model in simulation.

where t_{ob} is the time instant when the elevator reflex is switched on, the symbol "+"/“-” represents the time just before/after the reflex is triggered. Also note that y_1 in (10) is set at -1 because the retraction of the swing leg requires the reversal of the angular velocity.

The LC enlarges the ground clearance with smooth variation of the corresponding coefficients within the time interval T_s by

$$\begin{cases} g_i^{sw+} = g_i^{sw-} + \Delta g_i^{sw} \min \left(1, \frac{t-t_{ob}}{T_s} \right) \\ h_i^{sw+} = h_i^{sw-} + \Delta h_i^{sw} \min \left(1, \frac{t-t_{ob}}{T_s} \right) \end{cases} \quad (11)$$

where Δg_i^{sw} , Δh_i^{sw} are the adjustable increments associated with the higher ground clearance in stage II, and $i \in \{\beta, \gamma\}$. Fig. 7 shows the CPG outputs with the elevator reflex triggered at $t = 0.7$ s. The leg prolongs its swing phase and recovers its normal stance phase by the end of the elevator reflex at touchdown.

Fig. 8 shows the foot pathway of the elevator reflex suffering arbitrary step obstacles. The reflex is triggered on at $t_{ob} = 0.3$ s, 0.5 s, 0.7 s and 0.9 s in sequence. All the pathways complete the retraction with sufficient ground clearance and attain the nominal AEP regardless of the variation of the step obstacles.

4.2. Searching reflex generation

The searching reflex is related to the detecting movements that seek available foothold when encountering gap, ditch or hole. Herein the searching reflex is defined from the perspective of engineering realization and distinguished from the academic definition in biology study. The searching behavior with high frequency is realized through the coordination of three joints of leg. The swing phase has to be prolonged in order that the off-ground foot could afford continually seeking actions. The searching reflex is switched on when the following conditions hold simultaneously.

- The leg approaches the end of swing, namely $x_1 > 0 \cap \dot{x}_1 = 0$.
- The foot does not get ground support yet, which indicates $F_{toe-z} < F_{contact-z}$.

As shown in Fig. 9, the foot protracts with relatively small amplitude and high frequency around the current AEP to dig into the unknown circumstance until it reattains an effective support. An exception must be declared that the foot will return to its initial AEP waiting for high-level regulation if no support site appears during searching.

The searching reflex can be regarded as a series of periodic oscillations with varied amplitudes and frequencies. In order to achieve such oscillation with the higher frequency and smaller amplitude, we decelerate the movement of α -joint, and meanwhile accelerate β - and γ -joint through modulating the natural frequency of the VDP model as

$$\begin{cases} \omega_1(t_{td}^+) = 0.5\omega_1(t_{td}^-) \\ \omega_2(t_{td}^+) = 1.5\omega_2(t_{td}^-) \\ \omega_3(t_{td}^+) = 1.5\omega_3(t_{td}^-) \end{cases} \quad (12)$$

where t_{td} is the time instant when the searching reflex is triggered. Note that the original leader-follower coupling terms between \mathbf{z}_1 and \mathbf{z}_2 , \mathbf{z}_3 in (5) is unnecessary since the frequency ratio among the three neurons $\omega_1 : \omega_2 : \omega_3$ has been updated from $1 : 2 : 2$ into $1 : 6 : 6$. Therefore the coefficients k_{12} and k_{13} should be set to zero such that the original CPG network in searching reflex will be updated as

$$\begin{cases} \dot{x}_1 = y_1 \\ \dot{y}_1 = -\varepsilon_1(b_1x_1^2 - 1)y_1 - \omega_1^2(t_{td}^+)x_1 \\ \dot{x}_2 = y_2 \\ \dot{y}_2 = -\varepsilon_2(b_2x_2^2 - 1)y_2 - \omega_2^2(t_{td}^+)x_2 + k_{32}(y_3 - y_2) \\ \dot{x}_3 = y_3 \\ \dot{y}_3 = -\varepsilon_3(b_3x_3^2 - 1)y_3 - \omega_3^2(t_{td}^+)x_3 + k_{23}(y_2 - y_3) \end{cases} \quad (13)$$

Note that we preserve the mutual coupling term $k_{32}(y_3 - y_2)$ and $k_{23}(y_2 - y_3)$ for neuron oscillator \mathbf{z}_2 and \mathbf{z}_3 to maintain the phase-locked property between these two neurons as previously devised in the original CPG network (5).

The associated LC will be accordingly adapted so as to produce a relatively slow movement for α -joint, and relatively fast

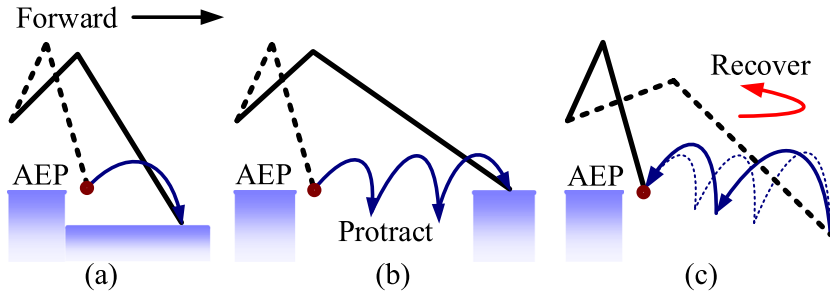


Fig. 9. Schematic of the searching reflex. (a) one step searching. (b) multi-step searching. (c) recover with no available foothold. Source: Adapted from [27].

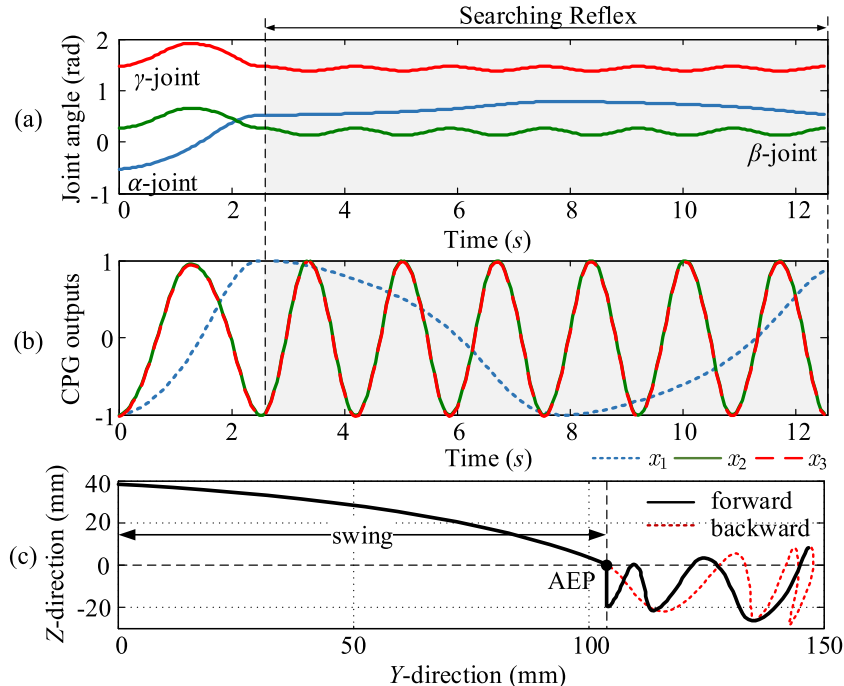


Fig. 10. Numerical result of the searching reflex. (a) the joint angles; (b) the CPG outputs; (c) the foot trajectory on Y-Z plane ($\sigma = 1.2$). See Section 6.1 for the structural specifications for the virtual hexapod model in simulation.

searching movements for β - and γ -joint. The update law of the coefficients are given by

$$\begin{cases} \alpha(t_{td}^+) = -\Delta\alpha x_1 + \alpha(t_{td}^-) + \Delta\alpha \\ \beta(t_{td}^+) = -\mu\Delta\beta x_2 + \beta(t_{td}^-) - \Delta\beta \\ \gamma(t_{td}^+) = -\mu\Delta\gamma x_3 + \gamma(t_{td}^-) - \Delta\gamma \end{cases} \quad (14)$$

where $\Delta\alpha$, $\Delta\beta$ and $\Delta\gamma$ are the searching oscillation amplitudes for α -, β - and γ -joint, respectively; μ is the coefficient of adjusting the searching amplitude, and is formulated as

$$\mu = 0.5(\sigma - 1)x_1 + 0.5(\sigma + 1) \quad (15)$$

Here $\sigma > 1$ is a constant that restricts the adjustment coefficient μ within the range $[1, \sigma]$, providing a deeper detection depth as the hip joint moving forward.

According to the mechanical structure of the robotic leg, $\Delta\alpha$, $\Delta\beta$ and $\Delta\gamma$ are set at 7.5° , 4° and 2.5° , respectively. Fig. 10 shows the numerical results of the searching reflex begins at the end of a nominal swing. Fig. 10(a) shows individual joint trajectories during searching reflex after triggered time $t_{td} = 2.5s$. The oscillation with lower frequency for α -joint and higher frequencies for β - and γ -joint are governed by the CPG outputs (see Fig. 10(b)) together with the updated LC. Fig. 10(c) shows the

searching behavior after the foot reaches its conventional AEP. Due to the frequency ratio $\omega_1(t_{td}^+) : \omega_2(t_{td}^+) : \omega_3(t_{td}^+) = 1 : 6 : 6$, the toe repeats 3 periods for searching forward and backward. It is clear to see that the oscillation amplitude turns larger as the searching digs deeper, which is thanks to the update law (14) of the coefficients in LC. Once the toe attains a new feasible foothold to support, the searching reflex is immediately terminated and this involved leg will switch into stance phase from the prolonged swing phase.

5. Establishment of locomotion control framework for hexapod walking robot

5.1. General control framework

The locomotion control framework for hexapod walking robot is established as illustrated in Fig. 11. The movement of each leg is governed by only one CPG controller. A finite state machine (FSM) is introduced to allocate the swing/stance phase of each leg according to the discrete event such as leg touchdown, lift-off. Since the walking pattern of the hexapod walking robot is determined by the movements of α -joint in each leg, the FSM could regulate the waveform of the leader neuron z_1 in each

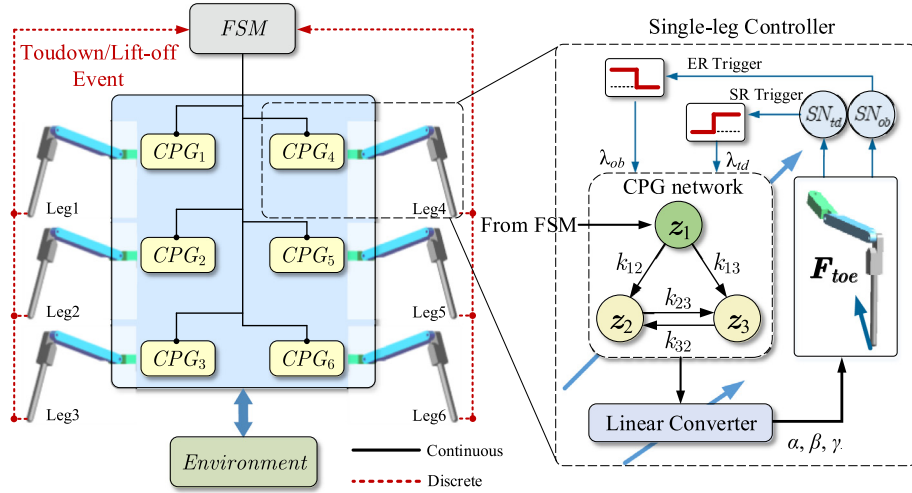


Fig. 11. The schematic of the locomotion control framework for the hexapod walking robot. The FSM allocates the swing/stance movement of each leg based on the received discrete touchdown/lift-off event. The partial view illustrates the details inside the single-leg controller which consists of the CPG network, the linear converter as well as two sensory neurons to transfer the tactile sensing data \mathbf{F}_{toe} into the trigger signals (λ_{ob} and λ_{td}) that are utilized to execute the controller switching. The diagonal arrows indicate that the CPG network together with the linear converter is switchable according to the trigger signals.

CPG network by pre-setting the initial conditions at $[-1, 0]^T$ for Leg1, Leg3, Leg5 and $[1, 0]^T$ for Leg2, Leg4, Leg6. The CPG network (5) works in conjunction with the LC (6) to produce nominal leg movement on flat ground. The tactile information of toes are monitored by the sensory neuron SN_{ob} and SN_{td} . The elevator and searching reflex will be switched on according to the unit step impulse of the corresponding signal λ_{ob} and λ_{td} , altering the coefficients of the single-leg controller to provide reactive activities in dealing with unexpected terrains. To be more specific, the trigger signal λ_{ob} and λ_{td} are treated as the switching flag to select the corresponding single-leg controller (namely, the phase regulator and the linear converter) when the single leg encounters the unexpected terrain profiles. The fundamental mechanism of this sensory feedback-based network switching in the FSM obeys the following rules.

- Case I (nominal walking): the regular CPG network (3) will be employed as the phase regulator, working in conjunction with the corresponding linear converter (4) to produce nominal leg movement in tripod gait with $\lambda_{\text{ob}} = 0$ and $\lambda_{\text{td}} = 1$ on flat ground.
- Case II (elevator reflex triggered): the rising jump of $\lambda_{\text{ob}}(0 \rightarrow 1)$ triggers the elevator reflex, which causes the update of the network state by using (8) and the corresponding linear converter by using (9) to generate an upward stroke in order to overpass the obstacle the leg encounters.
- Case III (searching reflex triggered): the falling jump of $\lambda_{\text{td}}(1 \rightarrow 0)$ triggers the searching reflex, which causes the update of the CPG network from (3) into (11) by adjusting the natural frequency of the coupled neuron oscillators with (10), and the corresponding linear converter from (4) into (12) with (13) to generate repeatable downward searching reactions for available foothold.

It is clear that the sensory feedback pathway plays a critical role in enhancing the adaptability of the CPG network-based single-leg controller in dealing with terrain disturbances.

5.2. Finite state machine

In the traditional tripod gait, the legs can be naturally divided into two groups, namely, {Leg1, Leg3, Leg5} and {Leg2,

Leg4, Leg6}. The legs in the identical group maintain synchronized movements (i.e., swing/stance), vice versa, the legs in the alien-group display the opposite movements (i.e., stance/swing). The FSM applied here works as a “virtual clock” to synchronize individual legs (especially those legs suffering from abnormal terrain disturbances to trigger local reflex reactions), providing a relatively safe liftoff condition during each walking stride for all legs. However the high-level commands (such as the desired walking speed, gait patterns as well as the routine orders) are conventionally customized and are beyond the utility of the FSM in this paper. Considering that either the elevator reflex (ER) or the searching reflex (SR) could be momentarily triggered during walking on irregular terrain, a novel FSM-driven tripod gait for hexapod walking robot is proposed by virtue of creating the additional “Swing/Stance Prolong” state to the original “Swing/Stance” state in the FSM as illustrated in Fig. 12.

The Swing/Stance Prolong state refers to the situation that the leg accomplishes or aborts its swing/stance phase and retains the current posture still to await until all legs get footholds. Particularly, the state switching routine to Swing/Stance always occurs as the condition ATD is achieved. For an individual leg, the current stance will be terminated when at least one leg from the alien group touches ground, which is defined as the condition “aTD”. In order to deal with the interruption caused by unexpected disturbance during the tripod gait cycle, the FSM synchronizes the legs by enforcing the leg on the ground come into the Swing/Stance Prolong state until the leg executing local reflex reaches the touchdown state. The operation mechanism of the FSM is listed in Table 2. Herein the symbol “ \cap ” indicates the logical conjunction (Boolean “AND” operator).

6. Simulation and experiment results

6.1. Simulation results

The simulation on a virtual model is conducted to testify the performance of the proposed locomotion controller in generating adaptive tripod gait pattern as well as treating terrain perturbations by using the presented local reactive mechanisms. The virtual model together with the irregular terrains is created in MSC.ADAMS software. The proposed locomotion control framework including the FSM as well as the CPG network integrated with two local reaction mechanisms is fulfilled in

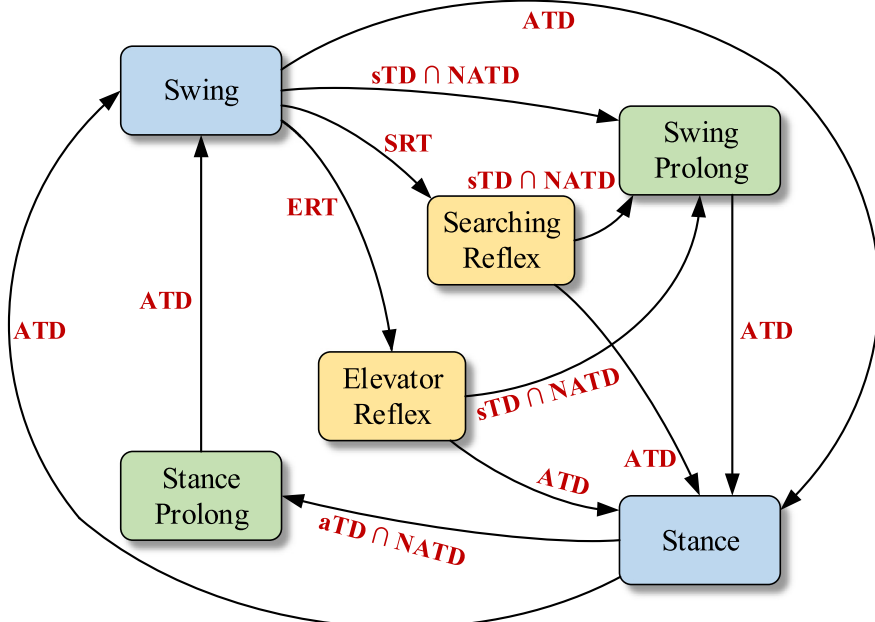
**Fig. 12.** The event-based FSM.

Table 2
Operation mechanism of the FSM.

Abbr.	Condition	Event descriptions
ERT	$\lambda_{ob}^i = 1$	Elevator Reflex Triggered ER is switched on.
SRT	$\lambda_{td}^i \cap x_i > 0 \cap \dot{x}_i = 0$	Searching Reflex Triggered Triggered SR is switched on.
ATD	$\sum_{i=1}^6 \lambda_{td}^i = 6$	All legs Touchdown All six legs contact with ground.
NATD	$0 < \sum_{i=1}^6 \lambda_{ob}^i < 6$	Not-All legs Touchdown At least one leg is in aerial.
sTD	$\lambda_{td}^i = 1$	Self Touchdown The leg itself contacts with ground.
aTD	$\sum_i \lambda_{td}^i \geq 1, i \in \text{alien group}$	Alien-group leg Touchdown At least one leg in alien-group contacts with ground.

Table 3
Structural specifications of the virtual hexapod model in simulation.

Description	Value	Description	Value
Coxa length	50 mm	Body length	250 mm
Thigh length	120 mm	Body height	120 mm
Shank length	150 mm	Foot clearance	40 mm

MATLAB/Simulink environment, which generates the movement commands for individual joints of the robot during the MATLAB-ADAMS co-simulation process at 1 kHz. The kinematical information (i.e., joint angle/torque, body posture) together with the tactile sensing during foot-ground interaction are simultaneously recorded throughout simulation. The robot is not aware of the *ground truth*, exhibiting “blind walking” for all scenarios as shown in Fig. 13. The structural specifications of the virtual hexapod model are collected in Table 3.

6.1.1. Elevator reflex simulation

The first scenario as shown in Fig. 13(b) is created to examine the performance of the robot with elevator reflex behavior, a 40 mm height obstacle is located on the right side of the even surface. In simulation, the parameters of the CPG network are listed in Table 1. According to the natural frequency $\omega_1 = 0.4\pi$,

the nominal cycle of the FSM-driven tripod gait is fixed at $T = 5$ s. The contact force detection threshold $F_{contact-x}$ and $F_{contact-y}$ are set at 10 N for all legs. The regenerated ground clearance produced by the linear converter (6) is set at 80 mm (200% of the obstacle height).

Fig. 14(a) shows the snapshots when the robot walks across the step obstacle. The legs on the right side will encounter the obstacle during swing to trigger the elevator reflex. The swing phase of the involved leg is lengthened to generate the re-planning trajectory with a higher ground clearance as illustrated in Fig. 14(b). Therefore executing these reactive behaviors will definitely change the scheduled gait pattern. However, the FSM-driven tripod gait will overcome this disadvantage by adding the swing/stance prolong state to the legs without interruption in gait cycle. The contact is detected by setting the force threshold at 10 N in simulation. As shown in Fig. 14(c), the elevator reflexes are successively triggered at $t = 10.5$ s with contact force 55.6 N for Leg4, $t = 14.2$ s with 62.4 N for Leg5 and $t = 18.4$ s with 85.5 N for Leg6. The transition curve between the nominal swing curve and regenerated trajectory prevents the leg from stumbling by the step obstacle and provides sufficient ground clearance for each leg to cross over successfully. It is worth noting that one may appropriately modulate the parameters of LC within the feasible working space of individual joints in order to obtain

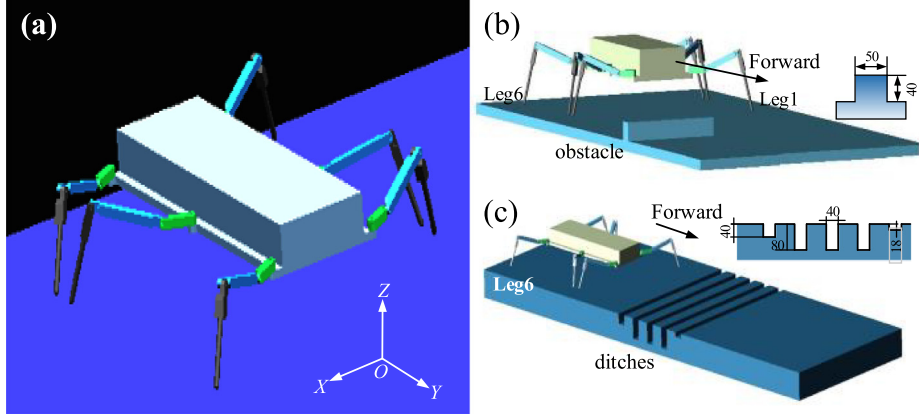


Fig. 13. Simulation setup. (a) the virtual hexapod model. (b) the scenario created for testing the elevator reflex behavior. (c) the scenario created for testing the searching reflex behavior.

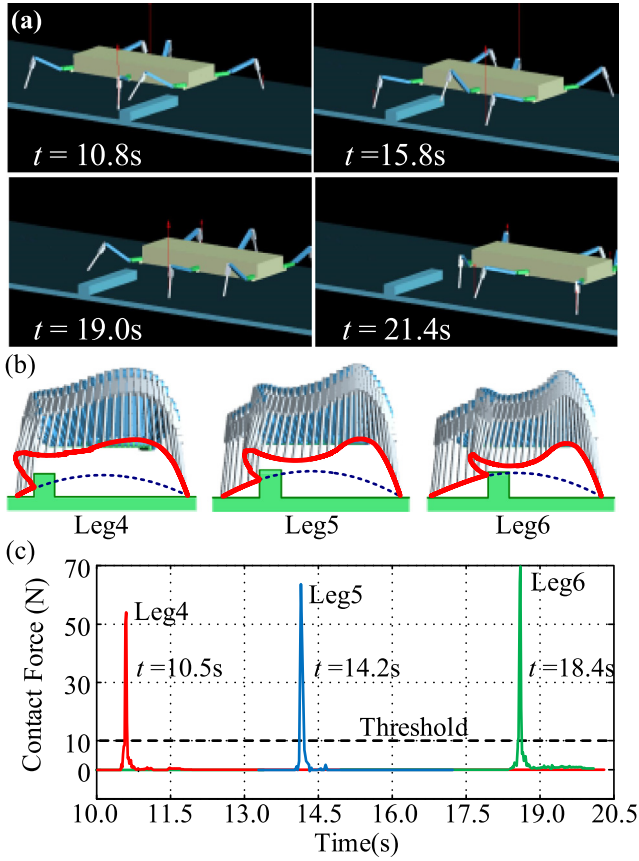


Fig. 14. Simulation results for executing elevator reflex. (a) snapshots of the robot walks across the step obstacle.(b) leg trajectories on the sagittal plane. (c) sampled contact forces of individual toes.

higher effective ground clearance to swing across different step obstacles.

6.1.2. Searching reflex simulation

The second scenario as shown in Fig. 13(c) wherein the striped-like terrain with ditches in different depth is arranged to examine the proposed CPG controller with the searching reflex mechanism. The parameters of the CPG network is the same as used in the previous simulation. The oscillation amplitudes of the LC are set at $\Delta\alpha = 7.5^\circ$, $\Delta\beta = 4^\circ$ and $\Delta\gamma = 2.5^\circ$. The constant $\sigma = 1.2$ is used to provide a detection depth roughly

between 0 to 28 mm. The vertical contact force threshold $F_{contact-z}$ is set at 2 N to judge whether or not the foot touches ground. In order to testify the performance of the searching reflex in dealing with ditches at different depth, we parameterize the ditch into three categories: (a) small ditch (18 mm) for just a single-step searching; (b) medium ditch (40 mm) for multi-step searching; (c) large ditch (80 mm) that exceeds the feasible searching range.

Fig. 15(a) and (b) show the movement details of the searching reactive behavior observed in simulation. The reactive behavior is terminated once the toe gets foothold. Fig. 15(c) illustrates the stick diagram of the gait pattern, revealing the operation mechanism of the FSM-driven tripodod gait with searching reflex. The red arrow indicates that the leg in conventional swing/stance phase is aborted and enforced into the corresponding swing-/stance-prolong phase scheduled by the FSM. It is obvious to see that the swing-stance transition always appears at ATD state while the searching reflex is always triggered at the end of swing. Compared with the maximal detection depth at 28 mm, the ditch at 80 mm depth can be regarded as an unfeasible groove for touchdown while the ditch at 18 mm is within the feasible searching range of single leg. All legs recover to the synchronized state when the leg in searching ultimately obtains foothold (at $t = 3.8$ s, 7.5 s, 11.2 s, 14.5 s and 17.5 s). Also note that the searching reflex will inevitably alter the AEP (where the toe loses support at touchdown) since a new detected foothold emerges. This variation of AEP will further affect the PEP during the forthcoming stance phase, and can be corrected in the next swing phase due to the preservation of the AEP from the single-leg controller.

6.2. Experiment results

6.2.1. The hexapod prototype

We further implement the experiments with the self-developed hexapod robot as shown in Fig. 16 to verify the performance of the proposed locomotion controller with local reactive behaviors. The robot has 18 active rotary joints driven by BLDC motor (MAXON EC60 for β -joint, EC45 for α - and γ -joint) with the structural specifications collected in Table 4(see Ref [37] for details of the mechanical structure information). The foot is equipped with F/T sensor (ATI-FT11293 with the tangential capacity $660 \text{ N} \pm 1\% \text{ F.S.}$ and the normal capacity $2000 \text{ N} \pm 1\% \text{ F.S.}$) to detect foot-ground contact as well as obstacle encountering during the swing pathway. Particularly, a special passive compliant ankle as shown in the partial view of Fig. 16 is mounted between the toe and the shank for each leg. A spherical hinge is arranged to connect the rubber foot pad and the ankle such that

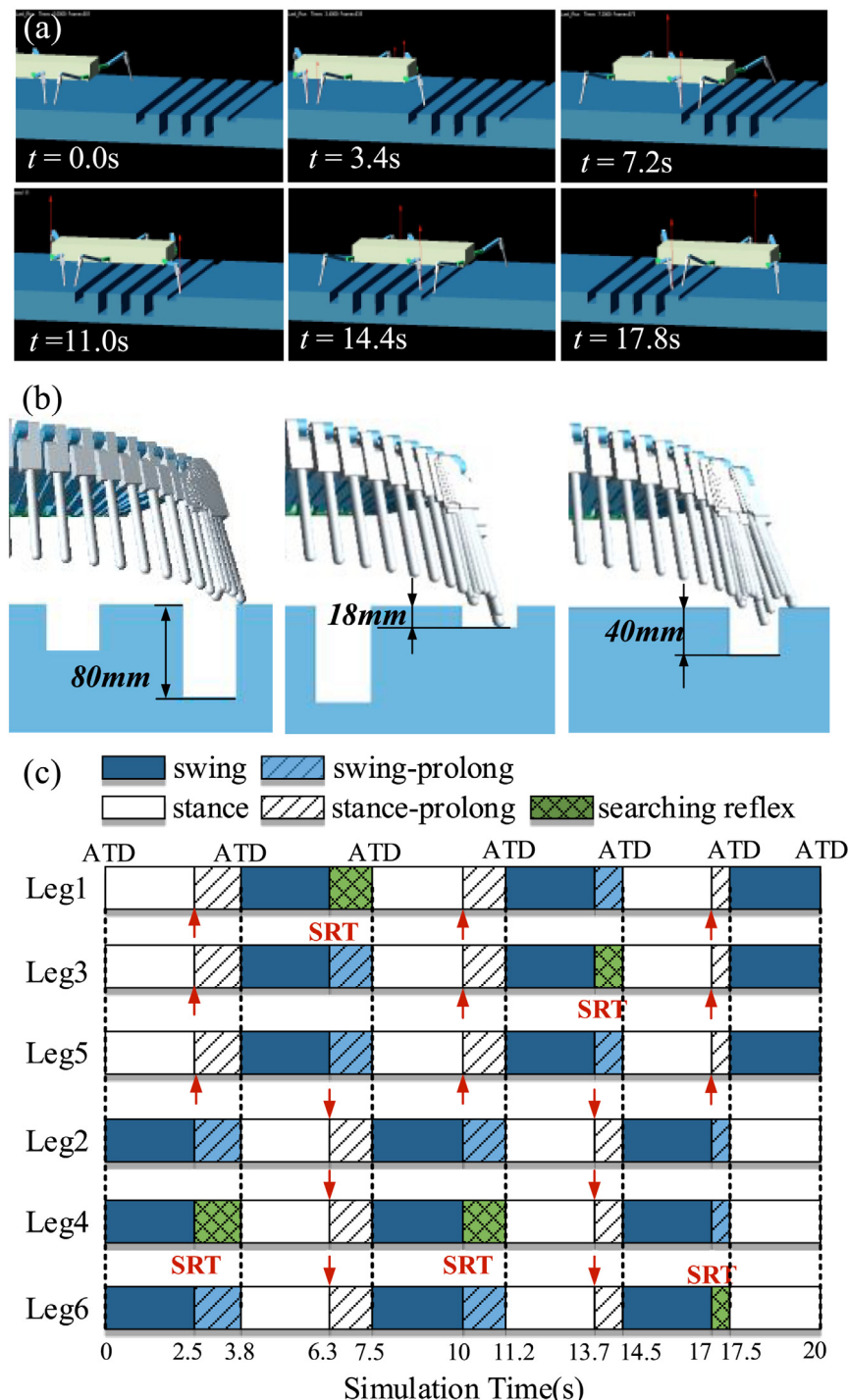


Fig. 15. Simulation results for executing searching reflex. (a) snapshots of the robot traverses ditches. (b) leg trajectories on the sagittal plane. (c) stick diagram of the simulated gait pattern.

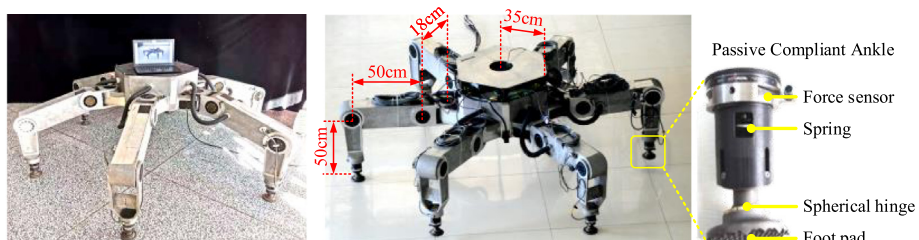


Fig. 16. The hexapod prototype used in the experimental validation.

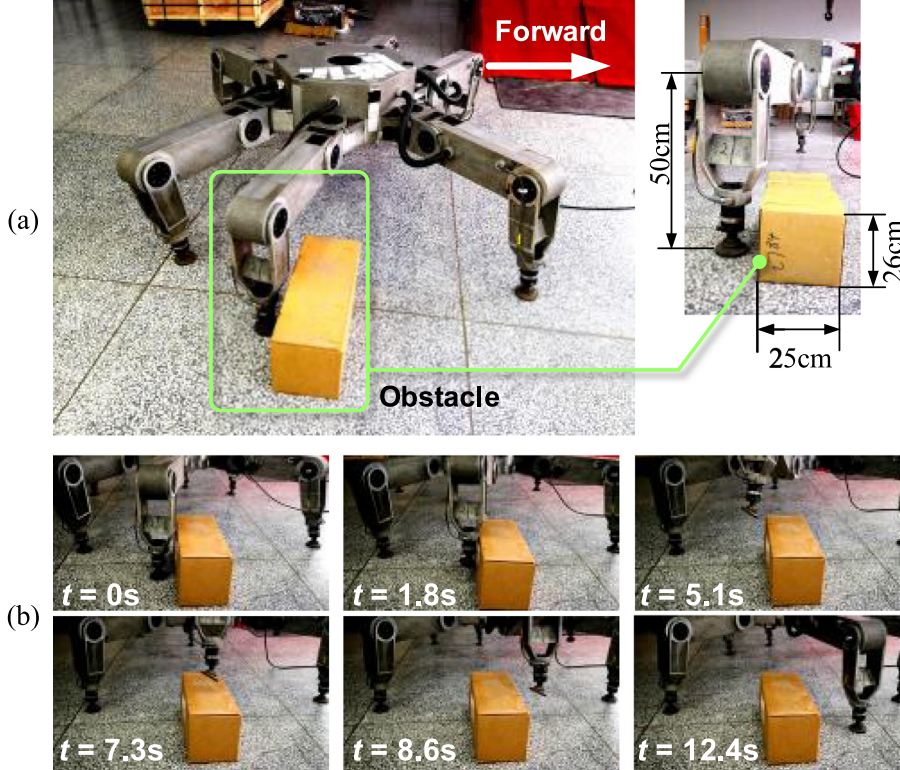


Fig. 17. Experiment setup and snapshots for walking test with elevator reflex behavior. (a) experiment arrangement. (b) snapshots of the walking hexapod traversing step obstacle with triggered elevator reflex behavior.

the foot could passively adapt the uneven terrain without causing motion interference during stance phase. A gauged linear spring is also installed inside the ankle housing to connect the force sensor. The purpose of equipping this passive compliant structure onto the foot is to ameliorate unexpected foot-ground interaction caused by terrain irregularities. The actual foot-ground contact condition is estimated by sampling the F/T sensor at 1 kHz with intercepted filter-like threshold value for tangential and normal direction, respectively such that misjudgment of foot-ground contact due to the signal noise will be alleviated.

6.2.2. Walking test with elevator reflex behavior

The experimental setup is shown in Fig. 17(a) where a step obstacle with height 25 cm and width 26 cm is arranged in the pathway of the middle leg of the robot. The obstacle is made of the steel ingot wrapped in carbon box and weights 45 kg roughly to provide firmly standing in presence of the foot collision. The nominal ground clearance of the single-leg in swing phase is pre-set at 24 cm with AEP and PEP fixed at 15 cm and -15 cm (measured with respect to the upper body coordinate), respectively. The robot executes tripod gait pattern without being aware of the ground truth knowledge throughout the experiment. Fig. 17(b) shows the snapshots of the robot encounters the obstacle and then successfully walks over it with the devised elevator reflex behavior as expected.

To better reveal the operation mechanism of the proposed elevator reflex, the contact force component $|F_{toe-x}|$, $|F_{toe-y}|$ and $|F_{toe-z}|$ of the leg involved are shown in Fig. 18 with partial views to observe the details of the tactile sensing data. The detection threshold $|F_{contact-x}|$ and $|F_{contact-y}|$ in this scenario are set at 30 N. The middle leg starts at swing stride and the elevator reflex is triggered on at approximately $t = 1.85\text{ s}$ right after the contact force $|F_{toe-y}|$ exceeds the threshold as shown in the partial view (left). In contrast to the impulsive collision force (peak value

Table 4
Structural specifications of the hexapod prototype.

Description	Value	Description	Value
Coxa length	180 mm	Coxa mass	3.58 kg
Thigh length	500 mm	Thigh mass	22.14 kg
Shank length	500 mm	Shank mass	7.19 kg
Foot length	25 mm	Foot mass	0.2 kg
Body height	500 mm	Body mass	121.9 kg

for $|F_{toe-x}|$, $|F_{toe-y}|$ and $|F_{toe-z}|$ are 3.91 N, 53.75 N and 22.41 N, respectively) observed during the toe touches the obstacle, the contact force maintains relatively small (less than 15 N for all contact force components) and stable for the normal swing movement as shown in the partial view (right), which provides a convenient and reliable judgment for executing toe-obstacle collision detection.

The foot trajectory during the elevator reflex reaction is shown in Fig. 19. The nominal ground clearance h_{\max} generated by the LC in the single-leg controller is 240 mm. By using the reflex action with adjustment law in (11), the middle leg rebounds and offers a higher ground clearance to walk astride the obstacle. Also note the updated trajectory that exhibits the elevator reflex reaction converges to the nominal AEP as scheduled at the end the prolonged swing phase, which is in consistent with the performance displayed by the virtual hexapod model in the previous simulation.

6.2.3. Walking test with searching reflex behavior

Another scene created for testing the performance of the hexapod robot with searching reflex behavior in terrain detection is shown in Fig. 20(a). A cliff-like obstacle (fibrous gypsum) with maximum height 150 mm is arranged in the right-side pathway of the hexapod robot. The tripod gait with the nominal stride length 100 mm is maintained throughout the walking test. For the

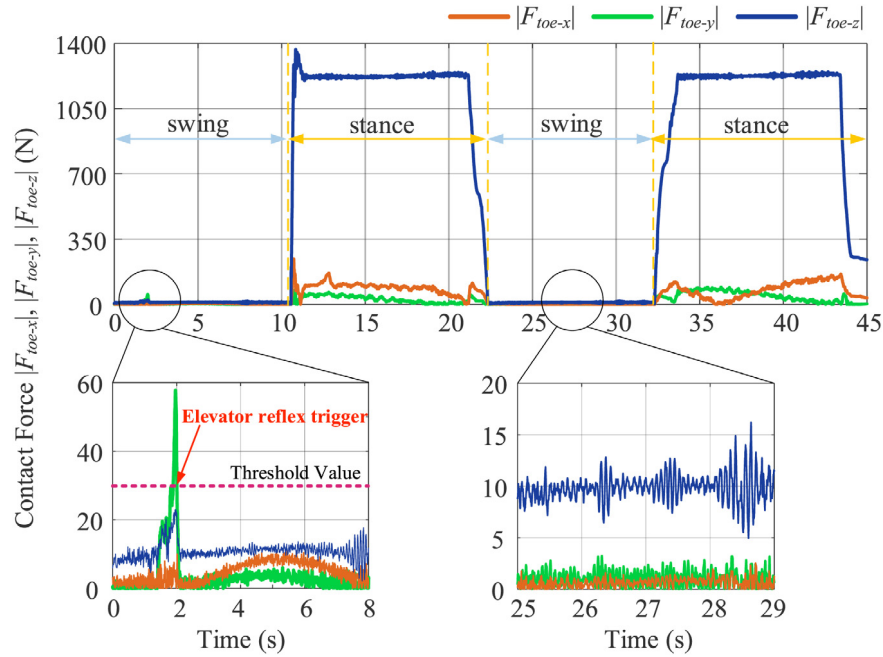


Fig. 18. Contact force of the middle leg recorded during the elevator reflex test. The partial views shows details of the tactile sensing data in the reflex action (left) and the normal swing (right), respectively.

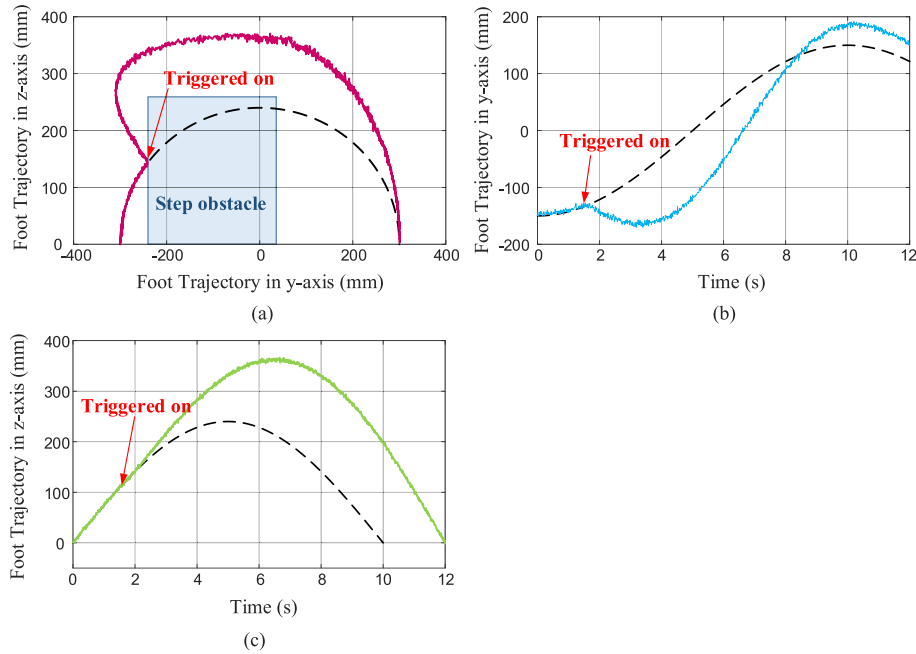


Fig. 19. Foot trajectory during the elevator reflex test. (a) foot trajectory on the sagittal plane. (b) foot trajectory versus time in y -axis. (c) foot trajectory versus time in z -axis. The dashed and solid line denote the nominal reference trajectory and the actual foot trajectory, respectively.

searching reflex, the maximum downward searching depth is set at 180 mm and the contact threshold value in z -direction is 30 N for the ground truth detection. Fig. 20(b) shows the snapshots of the middle leg seeking an available foothold after the searching reflex behavior is triggered on at $t = 20.8$ s approximately.

The corresponding contact force components F_{toe-x} , F_{toe-y} and F_{toe-z} of the middle leg during the walking test are shown in Fig. 21. The middle leg (on the right side of the robot with respect to the forward direction) steps on the arranged obstacle and then exhibits the foothold seeking via the proposed searching reflex in the forthcoming swing phase. The switch between the nominal swing and the sequent periodic seeking movement emerges at

the end of the nominal swing phase when the foot attains its AEP. It is clear to see that the contact force component F_{toe-z} roughly maintains at -4 N (much less than the pre-set contact threshold 30 N) as shown in the partial view of Fig. 21. The middle leg enlarges its seeking depth by using the LC proposed in (14) until the toe finally touches the ground at $t = 28.20$ s, which is in line with the quasi-periodic movement observed in Fig. 10. Note that the robot has no priori knowledge about the *ground truth* after the middle leg steps on the arranged obstacle. The adaptive behavior generated by the CPG network working in conjunction with the linear converter could effectively handle such uneven terrain with varied altitude (see Fig. 22).

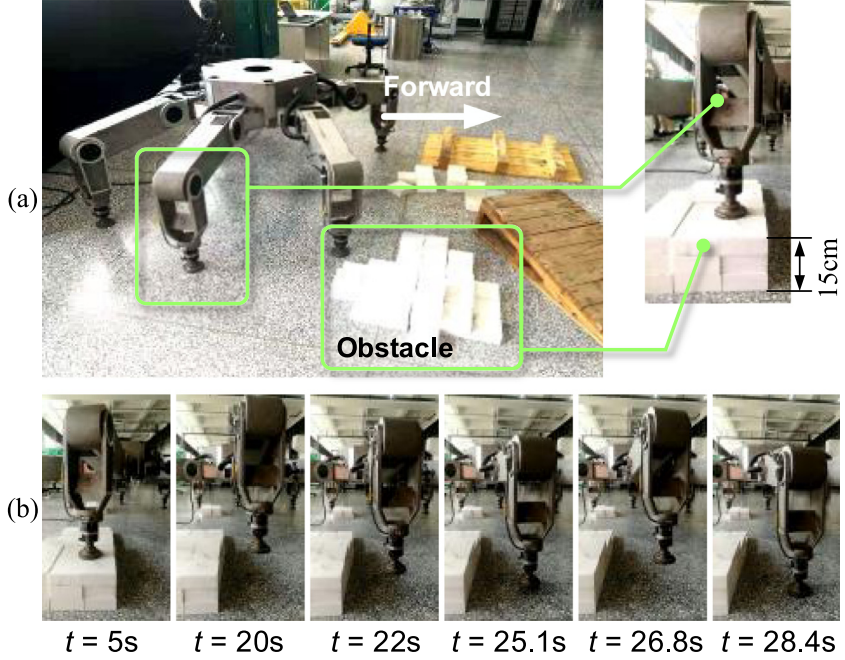


Fig. 20. Experiment setup and snapshots for walking test with searching reflex behavior. (a) experiment arrangement. (b) snapshots of the walking hexapod seeking for available foothold via the searching reflex behavior.

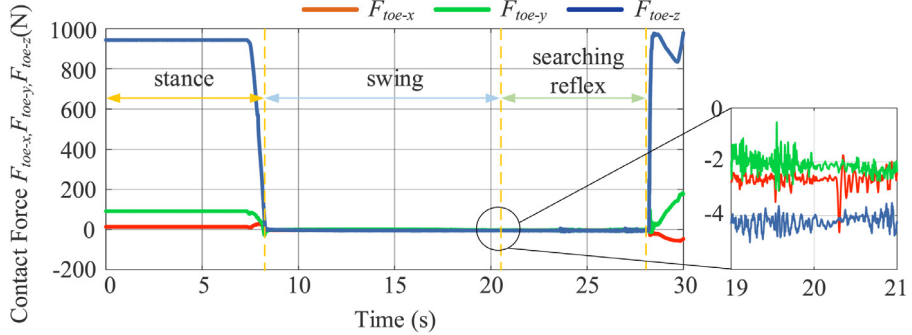


Fig. 21. Contact force of the middle leg recorded during the searching reflex test. The partial view shows the recorded force components when the searching reflex is triggered on.

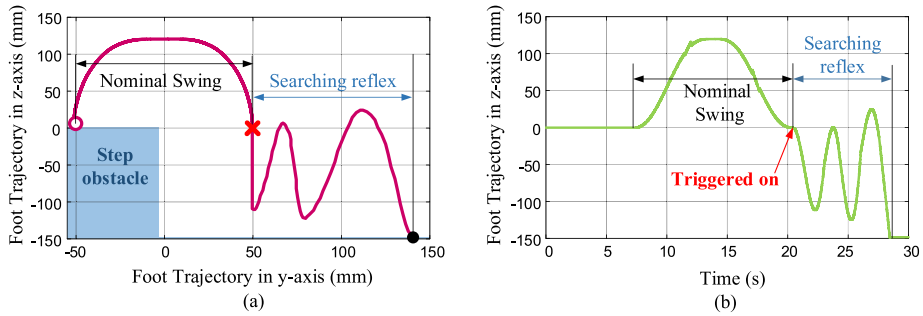


Fig. 22. Foot trajectory during the searching reflex test. (a) foot trajectory on the sagittal plane. (b) foot trajectory versus time in z-axis.

7. Discussions

7.1. Comparison with conventional CPG-based methods

Network coupling scheme has always been a crucial issue in the CPG-based control no matter what neuron model is used. How to systematically construct a CPG network capable of generating both rhythmical movement and adaptive behaviors is yet

unsettled. The main contribution of this paper is to present a simple but yet effective coupling scheme to construct a coupled CPG network composed of three VDP neurons as the single-leg controller wherein the local reflexes could be generated by either slightly changing the configuration or parameters of the controller, resulting adaptive behaviors in dealing with terrain disturbance for hexapod robot. To clarify the advantages of the

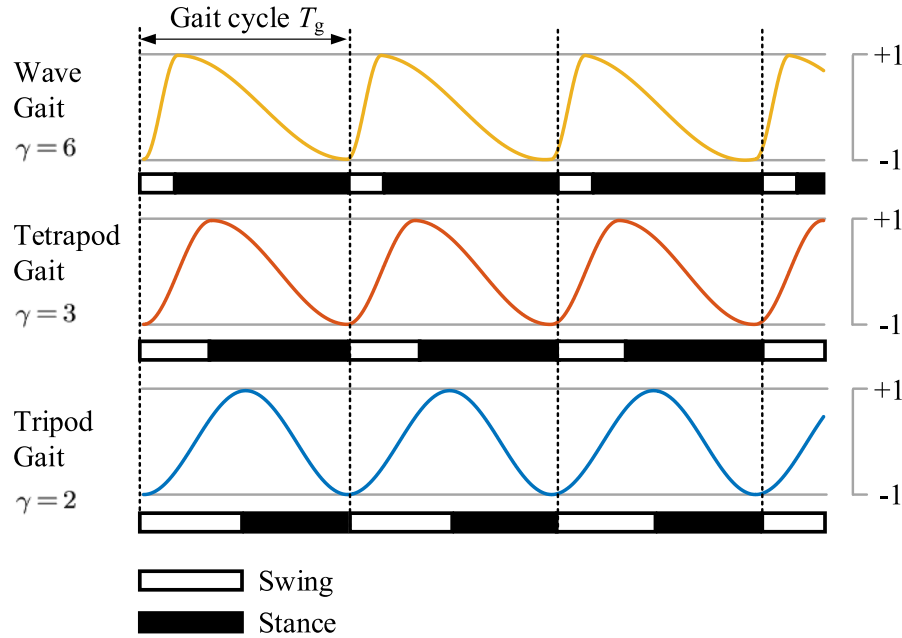


Fig. 23. Diverse gait pattern generation by using time-varying natural frequency of the VDP oscillator.

proposed method, a comprehensive comparison with the conventional CPG-based locomotion methods is implemented as shown in Table 5.

The superiority in tractability of the proposed CPG network with selectable waveforms gives the following conveniences in developing locomotion controller for legged robot. Firstly, the explicit tractability facilitates the task of leg movement planning, avoiding numerical process of parameter determination employed in the conventional methods listed in Table 5, which makes on-line adjustment possible. Additionally, decoupling the CPG signals from the kinematical correlation of specified robot type makes a step forward toward a potential versatile template applied in other robots with rhythmic movements.

7.2. Extensions to diverse gait patterns

Since the proposed CPG-based control framework could successfully generate the tripod gait pattern with adaptive local reaction behaviors provided by the reflex mechanisms. One interesting issue arises that what if using the CPG network to generate other possible gait patterns for hexapod robot? Generally speaking, the gait patterns of the hexapod robot is determined by the movements of individual body-coxa joint (α -joint) which is governed by the leader neuron z_1 for each coupled CPG network. In contrast to the constant natural frequency ω_1 in the original VDP oscillator utilized in Section 3.1, we could apply the following time-varying frequency adjustment law for the leader neuron z_1 of each leg as

$$\omega_1 = \begin{cases} \frac{\gamma\pi}{T_g}, & \text{swing phase} \\ \frac{\gamma\pi}{(\gamma-1)T_g}, & \text{stance phase.} \end{cases} \quad (16)$$

where T_g is the period of the gait cycle, γ is the gait indicator with $\gamma = 2, 3$ and 6 representing the tripod, tetrapod and wave gait, respectively. The corresponding gait patterns can be further extended from the traditional tripod gait to tetrapod gait and wave gait as illustrated in Fig. 23. The stick diagrams show the resulting gait patterns during the gait cycle for the hexapod walking robot.

It is worth noting that the proposed elevator and searching reflex mechanisms could be seamlessly replanted into the

"CPG network+FSM" architecture in both VDP oscillator with time-constant/varying natural frequency, which implies that the developed CPG-based locomotion control framework endows the capability of generating diverse gait patterns for the hexapod robot while preserving the local reactive behavior via sensory feedback.

7.3. Coupled CPG network vs sinusoids

Although there exists underlying connection between the sinusoids and the CPG network, the CPG network composed of VDP oscillators could not be replaced by serials of sinusoids in the locomotion control of legged robots. The characteristics comparison results are listed in Table 6 from the aspects of system formulation, stability, robustness as well as practical implementation. The fundamental distinction between the CPG network and the sinusoidal waves lies in the system configurations. The former is established by a group of coupled differential equations while the latter by a family of uncoupled explicit sinusoidal functions. The simple coupling scheme proposed in the single-leg controller guarantees the network could persistently output stable rhythmic pattern with/without perturbations. On the contrary, any variation of initial condition or state perturbation will definitely affect the synchronization of the waveforms of the sinusoids, and therefore interrupt the nominal leg movement. This is the weakness of the sinusoids employed in legged locomotion control when coping with terrain disturbances. Although what topology of the network or mathematical format of the waveforms is most suitable for legged locomotion control still remains open, the coupled CPG network in this study will be a better alternative for hexapod robot compared with the sinusoids.

8. Conclusions

In this paper, a CPG-based locomotion control method with local reactive behavior is presented for hexapod walking robot to enhance the adaptability when dealing with irregular terrains. We develop a two-layered CPG-based single-leg controller to produce nominal trajectory of each leg in tripod gait pattern. On the high-layer, the VDP oscillator is introduced to construct a

Table 5
Comparison with conventional CPG-based locomotion control methods.

Description	Proposed method	Ref. [25]	Ref. [38]	Ref. [39]
Neuron model	VDP oscillator	Matsuoka's oscillator	Matsuoka's oscillator	Hopf oscillator
Coupling scheme	Leader-follower coupling	Dual mutually chains	Holosymmetric connected	Unidirectional chain
Parameter tuning	Analytically determined	Experimentally determined	Partially obtained by hand tuning	Supervised learning
Adjustable profile of CPG output signals	Amplitude, frequency and phase lag (independently)	Amplitude and frequency (independently)	Amplitude and frequency (independently)	Amplitude frequency and phase lag (independently)
Usage of CPG outputs	Individual joint trajectories of single-leg	Switching desired hip angles and PD gains	Angular signals of hip joints	Reference trajectories of joints
Specified kinematical dependency	Decoupled	Coupled	Coupled	Decoupled
Application for locomotion control	Hexapodal walking	Quadrupedal Walking	Quadrupedal Walking	Limbless swimming
Local reactive behaviors achieved	Elevator and Searching reflex	Flexor, multiple stepping reflex	None	None

Table 6
Comparison between the CPG network and the sinusoids.

Description	CPG network	Sinusoids
System representation	Coupled differential equations	Explicit function
Steady state	Attractive limit cycle	Sinusoidal curve
Sensitivity to initial condition	Robust	Sensitive
Robustness to state disturbance	Yes	No
Practical implementation	4th-order Runge-Kutta solver	Direct coding

coupled neuron network that generates rhythmic signals with prescribed frequencies and phase-lags. The coupling scheme is carefully devised such that a “phase-locked” behavior is guaranteed amongst the leader and two follower neurons. On the low-layer, a linear converter transfers these resulting signals into the reference trajectories for individual legs. This two-layered controller decouples the mechanical dependence in terms of kinematical constraint of the robot from the establishment of the CPG network that solely works as a phase regulator, which endows this CPG network the potential of applying in locomotion control for other legged/legless robot.

We further propose two typical reactive behavior mechanisms including the elevator reflex and the searching reflex by using the proprioceptive sensing and the foot-ground tactile information as the sensory feedback. The FSM-driven locomotion control framework is constructed by combining the single-leg controller with two proposed reactive mechanisms. We implement simulation on a virtual model and experiments on a hexapod prototype to verify the effectiveness of the proposed locomotion control method. The robot with the elevator and searching reflex could successfully traverse irregular terrains, exhibiting a smooth walking performance in such unstructured environment.

The future work will direct towards the following aspects. First, the body posture (pitch, yaw, roll angle) will be embodied into the sensory feedback pathway in order to improve the adjustability in more challenge environment wherein terrain perturbations will be extended into discrete spatial obstacle as “forbidden zone” for robot to negotiate. Second, this CPG-based locomotion control framework will be integrated with the ability of generating diverse walking gait patterns with smooth transitions to enhance the mobility of the robot. At last but not least, the proposed CPG-based control method should be extended in generating omnidirectional walking movement for hexapod robot especially in outdoor environment to fully increase the practical application value of the proposed method.

Declaration of competing interest

The authors declare that they have no financial and personal relationships with other people or organizations that can inappropriately influence the work.

Acknowledgments

This work was supported in part by the National Key Research and Development Program of China (No. SQ2019YFB130016), the National Natural Science Foundation of China under Grant No. 51605115 and No. 91948202, Self-Planned Task (No. SKLRS201719A) of State Key Laboratory of Robotics and System (HIT), Open Projects (No. DMETKF2019013) of State Key Lab of Digital Manufacturing Equipment & Technology (HUST), Heilongjiang Postdoctoral Financial Assistance (LBH-Z16083) and Natural Science Foundation of Heilongjiang Province under Grant QC2017052.

References

- [1] T.I. Tóth, S. Daun, A kinematic model of stick-insect walking, *Physiol. Rep.* 7 (8) (2019) e14080, <http://dx.doi.org/10.14814/phy2.14080>.
- [2] C.J. Dallmann, V. Dürr, J. Schmitz, Motor control of an insect leg during level and incline walking, *J. Exp. Biol.* 222 (7), <http://dx.doi.org/10.1242/jeb.188748>.
- [3] D. Knebel, J. Wrner, J. Rillich, L. Nadler, A. Ayali, E. Couzin-Fuchs, The subesophageal ganglion modulates locust inter-leg sensory-motor interactions via contralateral pathways, *J. Insect Physiol.* 107 (2018) 116–124, <http://dx.doi.org/10.1016/j.jinsphys.2018.03.007>.
- [4] G.M. Nelson, R.D. Quinn, Posture control of a cockroach-like robot, *IEEE Control Syst. Mag.* 19 (2) (1999) 9–14, <http://dx.doi.org/10.1109/37.753930>.
- [5] R. Altendorfer, N. Moore, H. Komsuoglu, M. Buehler, H. Brown, D. McMordie, U. Saranli, R. Full, D. Koditschek, RHex: a biologically inspired hexapod runner, *Auton. Robots* 11 (3) (2001) 207–213, <http://dx.doi.org/10.1023/A:1012426720699>.

- [6] G.A.D. Lopes, B. Kersbergen, T.J.J. van den Boom, B. De Schutter, R. Babuška, Modeling and control of legged locomotion via switching max-plus models, *IEEE Trans. Robot.* 30 (3) (2014) 652–665, <http://dx.doi.org/10.1109/TRO.2013.2296105>.
- [7] M. Agheli, S.G. Faal, F. Chen, H. Gong, C.D. Onal, Design and fabrication of a foldable hexapod robot towards experimental swarm applications, in: 2014 IEEE International Conference on Robotics and Automation, ICRA, 2014, pp. 2971–2976, <http://dx.doi.org/10.1109/ICRA.2014.6907287>.
- [8] N. Kottege, C. Parkinson, P. Moghadam, A. Elfes, S.P.N. Singh, Energetics-informed hexapod gait transitions across terrains, in: 2015 IEEE International Conference on Robotics and Automation, ICRA, 2015, pp. 5140–5147, <http://dx.doi.org/10.1109/ICRA.2015.7139915>.
- [9] J. Chen, Y. Liu, J. Zhao, H. Zhang, H. Jin, Biomimetic design and optimal swing of a hexapod robot leg, *J. Bionic Eng.* 11 (1) (2014) 26–35, [http://dx.doi.org/10.1016/S1672-6529\(14\)60017-2](http://dx.doi.org/10.1016/S1672-6529(14)60017-2).
- [10] Y. Zhao, X. Chai, F. Gao, C. Qi, Obstacle avoidance and motion planning scheme for a hexapod robot Octopus-III, *Robot. Auton. Syst.* 103 (2018) 199–212, <http://dx.doi.org/10.1016/j.robot.2018.01.007>.
- [11] X. Xiong, F. Wrgtter, P. Manoonpong, Neuromechanical control for hexapedal robot walking on challenging surfaces and surface classification, *Robot. Auton. Syst.* 62 (12) (2014) 1777–1789, <http://dx.doi.org/10.1016/j.robot.2014.07.008>.
- [12] J. Dupeyroux, S. Viollet, J.R. Serres, An ant-inspired celestial compass applied to autonomous outdoor robot navigation, *Robot. Auton. Syst.* 117 (2019) 40–56, <http://dx.doi.org/10.1016/j.robot.2019.04.007>.
- [13] J. Dupeyroux, G. Passault, F. Ruffier, S. Viollet, J. Serres, Hexabot: a small 3D-printed six-legged walking robot designed for desert ant-like navigation tasks, in: IFAC Word Congress, 2017, pp. 1628–1631, <http://dx.doi.org/10.1109/ROBOT.2004.1307523>.
- [14] J. Dupeyroux, J.R. Serres, S. Viollet, AntBot: a six-legged walking robot able to home like desert ants in outdoor environments, *Sci. Robot.* 4 (2019) eaau0307, <http://dx.doi.org/10.1126/scirobotics.aau0307>.
- [15] J. Faigl, P. Čížek, Adaptive locomotion control of hexapod walking robot for traversing rough terrains with position feedback only, *Robot. Auton. Syst.* 116 (2019) 136–147, <http://dx.doi.org/10.1016/j.robot.2019.03.008>.
- [16] S. Grillner, T. Deliagina, A.E. Manira, R. Hill, G. Orlovsky, P. Wallén, Neural networks that co-ordinate locomotion and body orientation in lamprey, *Trends Neurosci.* 18 (6) (1995) 270–279, [http://dx.doi.org/10.1016/0166-2236\(95\)80008-P](http://dx.doi.org/10.1016/0166-2236(95)80008-P).
- [17] A. Büschges, Sensory control and organization of neural networks mediating coordination of multisegmental organs for locomotion, *J. Neurophysiol.* 93 (3) (2005) 1127–1135, <http://dx.doi.org/10.1152/jn.00615.2004>.
- [18] S. Grillner, P. Wallén, Cellular bases of a vertebrate locomotor system-steering, intersegmental and segmental co-ordination and sensory control, *Brain Res. Rev.* 40 (1) (2002) 92–106, [http://dx.doi.org/10.1016/S0165-0173\(02\)00193-5](http://dx.doi.org/10.1016/S0165-0173(02)00193-5).
- [19] K.G. Pearson, Generating the walking gait: role of sensory feedback, in: Brain Mechanisms for the Integration of Posture and Movement, in: Progress in Brain Research, vol. 143, Elsevier, 2004, pp. 123–129, [http://dx.doi.org/10.1016/S0079-6123\(03\)43012-4](http://dx.doi.org/10.1016/S0079-6123(03)43012-4).
- [20] W.A. Lewinger, R.D. Quinn, A hexapod walks over irregular terrain using a controller adapted from an insect's nervous system, in: 2010 IEEE/RSJ International Conference on Intelligent Robots and Systems, 2010, pp. 3386–3391, <http://dx.doi.org/10.1109/IROS.2010.5650200>.
- [21] B.L. Rutter, B.K. Taylor, J.A. Bender, M. Blümel, W.A. Lewinger, R.E. Ritzmann, R.D. Quinn, Descending commands to an insect leg controller network cause smooth behavioral transitions, in: 2011 IEEE/RSJ International Conference on Intelligent Robots and Systems, 2011, pp. 215–220, <http://dx.doi.org/10.1109/IROS.2011.6095030>.
- [22] B.L. Rutter, W.A. Lewinger, M. Blümel, A. Büschges, R.D. Quinn, Simple muscle models regularize motion in a robotic leg with neurally-based step generation, in: Proceedings 2007 IEEE International Conference on Robotics and Automation, 2007, pp. 630–635, <http://dx.doi.org/10.1109/ROBOT.2007.363057>.
- [23] D. Goldschmidt, F. Hesse, F. Wörgötter, P. Manoonpong, Biologically inspired reactive climbing behavior of hexapod robots, in: 2012 IEEE/RSJ International Conference on Intelligent Robots and Systems, 2012, pp. 4632–4637, <http://dx.doi.org/10.1109/IROS.2012.6386135>.
- [24] G. Li, H. Zhang, J. Zhang, H.P. Hildre, An approach for adaptive limbless locomotion using a cpg-based reflex mechanism, *J. Bionic Eng.* 11 (3) (2014) 389–399, [http://dx.doi.org/10.1016/S1672-6529\(14\)60052-4](http://dx.doi.org/10.1016/S1672-6529(14)60052-4).
- [25] H. Kimura, Y. Fukuoka, A.H. Cohen, Adaptive dynamic walking of a quadruped robot on natural ground based on biological concepts, *Int. J. Robot. Res.* 26 (5) (2007) 475–490, <http://dx.doi.org/10.1177/0278364907070809>.
- [26] T. Wang, W. Guo, M. Li, F. Zha, L. Sun, CPG Control for biped hopping robot in unpredictable environment, *J. Bionic Eng.* 9 (1) (2012) 29–38, [http://dx.doi.org/10.1016/S1672-6529\(11\)60094-2](http://dx.doi.org/10.1016/S1672-6529(11)60094-2).
- [27] K.S. Espenschied, R.D. Quinn, R.D. Beer, H.J. Chiel, Biologically based distributed control and local reflexes improve rough terrain locomotion in a hexapod robot, *Robot. Auton. Syst.* 18 (1) (1996) 59–64, [http://dx.doi.org/10.1016/0921-8890\(96\)00003-6](http://dx.doi.org/10.1016/0921-8890(96)00003-6).
- [28] R.D. Beer, J.C. Gallagher, Evolving dynamical neural networks for adaptive behavior, *Adapt. Behav.* 1 (1992) 91–122.
- [29] G. Endo, J. Morimoto, J. Nakanishi, G. Cheng, An empirical exploration of a neural oscillator for biped locomotion control, in: IEEE International Conference on Robotics and Automation, 2004. Proceedings, ICRA '04, vol. 3, 2004, pp. 3036–3042, <http://dx.doi.org/10.1109/ROBOT.2004.1307523>.
- [30] Y. Nakamura, T. Mori, M. aki Sato, S. Ishii, Reinforcement learning for a biped robot based on a CPG-actor-critic method, *Neural Netw.* 20 (6) (2007) 723–735, <http://dx.doi.org/10.1016/j.neunet.2007.01.002>.
- [31] S. Debnath, J. Nassour, G. Cheng, Learning diverse motor patterns with a single multi-layered multi-pattern CPG for a humanoid robot, in: 2014 IEEE-RAS International Conference on Humanoid Robots, 2014, pp. 1016–1021, <http://dx.doi.org/10.1109/HUMANOIDS.2014.7041489>.
- [32] M. Frasca, P. Arena, L. Fortuna, Bio-Inspired Emergent Control of Locomotion Systems, vol. 48, World Scientific, 2004, <http://dx.doi.org/10.1142/5586>.
- [33] U. Bässler, The femur-tibia control system of stick insects – a model system for the study of the neural basis of joint control, *Brain Res. Rev.* 18 (2) (1993) 207–226, [http://dx.doi.org/10.1016/0165-0173\(93\)90002-H](http://dx.doi.org/10.1016/0165-0173(93)90002-H).
- [34] U. Bässler, A. Büschges, Pattern generation for stick insect walking movements—multisensory control of a locomotor program, *Brain Res. Rev.* 27 (1) (1998) 65–88, [http://dx.doi.org/10.1016/S0165-0173\(98\)00006-X](http://dx.doi.org/10.1016/S0165-0173(98)00006-X).
- [35] H. Cruse, The control of body position in the stick insect carausius morosus when walking over uneven surfaces, *Biol. Cybernet.* 24 (1) (1976) 25–33, <http://dx.doi.org/10.1007/Bf00365591>.
- [36] K.G. Pearson, R. Franklin, Characteristics of leg movements and patterns of coordination in locusts walking on rough terrain, *Int. J. Robot. Res.* 3 (2) (1984) 101–112, <http://dx.doi.org/10.1177/027836498400300209>.
- [37] H. Gao, M. Jin, L. Ding, Y. Liu, W. Li, X. Yu, Z. Deng, Z. Liu, A real-time, high fidelity dynamic simulation platform for hexapod robots on soft terrain, *Simul. Model. Pract. Theory* 64 (2016) 125–145, <http://dx.doi.org/10.1016/j.simpat.2016.08.004>.
- [38] X. Zhang, H. Zheng, L. Chen, Gait transition for a quadrupedal robot by replacing the gait matrix of a central pattern generator model, *Adv. Robot.* 20 (2006) 849–866, <http://dx.doi.org/10.1163/15685530677681375>.
- [39] Y. Hu, J. Liang, T. Wang, Parameter synthesis of coupled nonlinear oscillators for CPG-based robotic locomotion, *IEEE Trans. Ind. Electron.* 61 (2014) 6183–6191, <http://dx.doi.org/10.1109/TIE.2014.2308150>.



Haitao Yu received the B.S., M.S. and Ph.D. degree in mechanical engineering from Harbin Institute of Technology (HIT), Harbin, China, in 2007, 2009, and 2014, respectively. He was a visiting scholar with the control system and robotics laboratory at the department of aerospace engineering, Ryerson University, Toronto, ON, Canada, from 2014 to 2015 before he joined HIT where he is currently working as a lecturer with the School of Mechatronics. His research interests include bio-inspired robots, legged locomotion control and underactuated systems.



Haibo Gao received the M.S. and Ph.D. degree in mechanical engineering from Harbin Institute of Technology (HIT), Harbin, China, in 1995 and 2003, respectively. He is now a Professor and Vice Dean in School of Mechatronics of HIT, and the Vice Dean of State Key Laboratory of Robotics and System of HIT. His research interests mainly focus on mobile robots, aerospace mechanism and control and multi legged robots.



Zongquan Deng received MS. Degree in mechanical engineering from the Harbin Institute of Technology (HIT), Harbin, China, in 1984.

In 1984, He joined the Department of Mechatronics, HIT, where he is currently the Vice President of HIT and the Director of National Defense Key Laboratory of Aerospace Mechanism and Control at HIT. His research interests include aerospace mechanism and control, mobile robots.